// Nanoscale

Accepted Manuscript

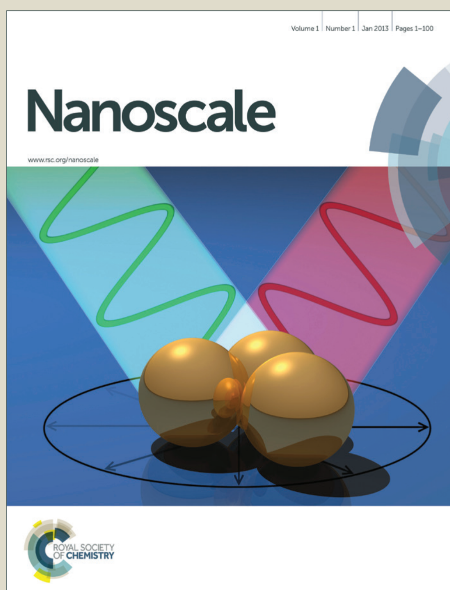

This is an *Accepted Manuscript*, which has been through the Royal Society of Chemistry peer review process and has been accepted for publication.

Accepted Manuscripts are published online shortly after acceptance, before technical editing, formatting and proof reading. Using this free service, authors can make their results available to the community, in citable form, before we publish the edited article. We will replace this *Accepted Manuscript* with the edited and formatted *Advance Article* as soon as it is available.

You can find more information about *Accepted Manuscripts* in the Information for Authors.

Please note that technical editing may introduce minor changes to the text and/or graphics, which may alter content. The journal's standard Terms & Conditions and the Ethical guidelines still apply. In no event shall the Royal Society of Chemistry be held responsible for any errors or omissions in this *Accepted Manuscript* or any consequences arising from the use of any information it contains.

ROYAL SOCIETY OF CHEMISTRY

www.rsc.org/nanoscale

CREATED USING THE RSC LaTeX PCCP ARTICLE TEMPLATE – SEE www.rsc.org/electronicfiles FOR DETAILS
ARTICLE TYPE
www. rsc.org/xxxxxx | XXXXXXXX

Transport limits in defect-engineered $LaAlO_3$/$SrTiO_3$ bilayers

Felix Gunkel,[*a] **Sebastian Wicklein,**[a] **Susanne Hoffmann-Eifert,**[a] **Paul Meuffels,**[a] **Peter Brinks,**[b] **Mark Huijben,**[b] **Guus Rijnders,**[b] **Rainer Waser,**[a] **and Regina Dittmann**[a]

Received Xth XXXXXXXXXX 20XX, Accepted Xth XXXXXXXXX 20XX
First published on the web Xth XXXXXXXXXX 200X
DOI: 10.1039/b000000x

The electrical properties of the metallic interface in $LaAlO_3$/$SrTiO_3$ (LAO/STO) bilayers are investigated with focus on the role of cationic defects in thin film STO. Systematic growth-control of the STO thin film cation stoichiometry (defect-engineering) yields a relation between cationic defects in the STO layer and electronic properties of the bilayer-interface. Hall measurements reveal a stoichiometry-effect primarily on the electron mobility. The results indicate an enhancement of scattering processes in as-grown non-stoichiometric samples indicating an increased density of defects. Furthermore, we discuss the thermodynamic processes and defect-exchange reactions at the LAO/STO-bilayer interface determined in high temperature equilibrium. By quenching defined defect states from high temperature equilibrium, we finally connect equilibrium thermodynamics with room temperature transport. The results are consistent with the defect-chemistry model suggested for LAO/STO interfaces. Moreover, they reveal an additional healing process of extended defects in thin film STO.

1 Introduction

The discovery of the conducting interface between the wide band gap perovskite insulators, $SrTiO_3$ (STO) and $LaAlO_3$ (LAO),[1] has sparked enormous scientific and technological interest. In analogy to similar interface effects in semiconductor heterostructures,[2] the supposed 2-dimensional electron gas (2DEG) formed at the LAO/STO interface represents a promising candidate system to emulate the achievements of semiconductor technologies in all-oxide devices.[3,4]
A general understanding of the conduction mechanism at oxide interfaces is an important prerequisite for the development of real electronic devices. Furthermore, it is desirable to obtain a transfer from the scientifically relevant *STO-single-crystal-based* LAO/STO interface to the technologically more relevant *STO-thin-film-based* interface system and superlattices. However, given the crucial impact of crystal defects on the electronic properties of LAO/STO interfaces,[5–15] the use of STO thin films adds new challenges to the field, namely understanding and controlling the defect structure of thin film STO. This is particularly important keeping in mind that electron transport along the LAO/STO interface actually takes place on the STO side of the interface.
Yet, conducting interfaces between thin film STO and LAO have been obtained for STO grown on a Si template[16] as well as for hetero- and homoepitaxial STO grown on perovskite templates.[6,17–19] However, their performance in terms of low temperature electron mobility is much lower than that of LAO/STO interfaces to single crystals.[16,17] This particularly hints at the presence of growth-induced defects in these samples. For thin film STO, cation non-stoichiometry and the associated appearance of cationic defects have been identified as crucial issues.[20–25] To date, however, cationic defects in STO have barely been considered as relevant defect species in the discussion of origin and appearance of the conducting interface between LAO and STO. Being acceptor-type defects, Sr-vacancies have been proposed to be responsible for the reduced electron density observed for LAO/STO interfaces after annealing in oxygen-rich atmosphere.[6] Moreover, the effect of *extrinsic* acceptor doping has been addressed by the insertion of single monolayers of chemically acceptor-doped STO close to the LAO/STO interface.[26,27] However, the influence of inherent *intrinsic* acceptor-type defects in thin film STO has not been considered so far.
Here, we follow the potential approach to alter the *intrinsic* cation stoichiometry in STO by growth-control. We investigated the electrical properties of LAO/STO bilayers comprising STO thin films grown under varied growth conditions. In particular, we varied the laser fluence, F, during the pulsed laser deposition (PLD) of the STO thin film. This procedure enables to continuously tune the composition of the STO thin film from being Sr-rich to stoichiometric to Ti-rich. The role of cationic defects for the electronic properties of LAO/STO interfaces is discussed from two perspectives, 1) thermodynamics and defect chemistry and 2) thin film growth. A combination of defect-engineering techniques for PLD-grown ox-

[a] *Peter Grünberg Insitut and Jülich Aachen Research Alliance - Fundamentals of Future Information Technology (JARA-FIT), Forschungszentrum Jülich GmbH, Jülich, Germany. Fax: +49 2461 612550; Tel: +49 2461 615339; E-mail: f.gunkel@fz-juelich.de*
[b] *MESA+ Institute for Nanotechnology, University of Twente, P.O. Box 217, 7500AE, Enschede, The Netherlands*

Nanoscale Accepted Manuscript

ide thin films and defect chemistry models of perovsikte oxide interfaces is then applied to understand and to control the electronic properties of LAO/STO bilayer interfaces.

2 General considerations on defects and thermodynamic processes in $SrTiO_3$

2.1 Point defects in $SrTiO_3$

Due to the essentially ionic character of strontium titanate point defects within the crystal lattice are generally charged rather than charge neutral. This results in a strong influence of the defect structure on the electronic properties of the nominal insulator STO. The most discussed defect species in STO are donor-type point defects, in particular *intrinsic* donors (oxygen vacancies, $V_O^{\bullet\bullet}$)* and *extrinsic* donors (e.g. lanthanum incorporated on Sr-sites, $La_{Sr}^{\bullet}$ or niobium on Ti-sites, $Nb_{Ti}^{\bullet}$). Donor-type defect states are commonly shallow in STO (i.e. they are located only a few meV below the conduction band edge), so that such defects are ionized at room temperature resulting in electronic conduction.

In STO, one has to consider acceptor-type defects, too. Besides *extrinsic* acceptor-doping, e.g. by doping Fe on Ti-sites ($Fe_{Ti}^{'}$), STO can generate *intrinsic* acceptors - namely cation vacancies - in analogy to intrinsic donors. † Specifically for STO, one has to consider doubly charged strontium vacancies ($V_{Sr}^{''}$) and four times negatively charged titanium vacancies ($V_{Ti}^{''''}$), while $V_{Ti}^{''''}$ are energetically less favorable than $V_{Sr}^{''}$.[29]

Cationic point defects form in thermodynamical (entropy-driven) processes as will be discussed in the following section. In the case of STO thin films, however, the role of cationic defects is further pronounced as they might moreover be induced and controlled in excess of their equilibrium concentrations during the growth process.

Energetically, acceptor-type defect states are usually located deep inside the band gap of STO. Therefore, *p*-type conduction is hardly observable in STO at room temperature as electron holes freeze out already above 300 K.

2.2 Defect chemistry of the LAO/STO interface

The equilibrium concentration of a defect species in a solid is determined by thermodynamics, i.e. the balance of energy (that it costs to generate the defect) and entropy (that is gained when generating the defect). As described by defect chemistry this yields in bulk STO a defined relation between electronic defects (electrons and holes) and ionic defects as a function of ambient oxygen partial pressure and temperature.[30] This textbook model is based on local charge neutrality and the appropriate thermodynamic representation of defect equilibria, i.e. mass action laws. In analogy to bulk STO, a defect chemical description of the LAO/STO-interface has been established, too.[5,6] In particular, it has been shown that the defect chemistry of the conducting LAO/STO interface follows the one of donor-doped bulk STO. Classically, this may be indicative for extrinsic doping, e.g. due to lanthanum intermixing across the LAO/STO interface (i.e. $La_{Sr}^{\bullet} > 0$). Compared to classical bulk STO, however, the complex nature of the LAO/STO interface might allow also for other donor-type doping mechanisms such as trapping of oxygen vacancies at the interface.[5,31] Moreover, charge is considered to be injected in absence of extrinsic or intrinsic defects as a result of the potential built-up caused by the polar nature of LAO.[7]

As we discuss below, the defect chemistry model established in Refs. 5,6 can be extended to a more general case accounting for the compensation of an internal electrical dipole. Charge transfer into the interface can (*in the simplest case*, i.e. assuming homogeneous charge injection) be formally modeled by a modification of the charge neutrality condition. Assuming that after charge transfer the STO close to the interface is no longer charge neutral, but carries an overall negative net charge $-Q_P$ (associated with charge density $-\rho_P$), the charge balance of the system is given by

$$p + 2\left[V_O^{\bullet\bullet}\right] - n - 2\left[V_{Sr}^{''}\right] - 4\left[V_{Ti}^{''''}\right] = -\rho_P,$$

where brackets indicate the concentration of a defect species and n, p display electron and hole concentrations. This equation is formally equivalent to the classical charge neutrality condition for donor-doped bulk STO (see Ref. 32). Hence, the assumption of polarity-induced charging of the LAO/STO interface returns a similar defect-chemistry as the assumption of extrinsic doping (in a formal treatment the various doping scenarios can therefore be summarized in a generalized charge density $\rho = \rho_P + [La_{Sr}^{\bullet}] + ...$). In other words: Independent of the particular nature of the donor-type doping process, the way strontium titanate deals with this extra charge remains the same. This generally implies two possible charge compensation mechanisms, 1) electronic charge compensation and 2) ionic charge compensation.[6,30,32] The first case may be seen as the more intuitive one. In fact, charge is compensated by free electrons. This is the generation of the 2DEG at the LAO/STO interface. The latter case is a competing charge compensation mechanism involving an activated Schottky equilibrium. It requires mobile strontium ions so that these can be removed from their lattice sites leav-

* In Kröger-Vink notation[28] the main index corresponds to the prevailing element sitting on a lattice site of the crystal. Vacancies are indicated by V. The subscript refers to lattice site of the original, perfect lattice. The superscript indicates the relative charge of a defect, with • indicating a positive relative charge, and ′ indicating a negative relative charge.

† Obviously, a missing cation cannot donate its electrons to the lattice (when forming a cation from the neutral atom). As a result, the total number of electrons (electron holes) in the system is reduced (increased) in presence of cation vacancies legitimating their classification as acceptor-type defects. Relative to the original lattice site, cation vacancies thus carry a negative net charge.

Nanoscale Accepted Manuscript

This journal is © The Royal Society of Chemistry [year]

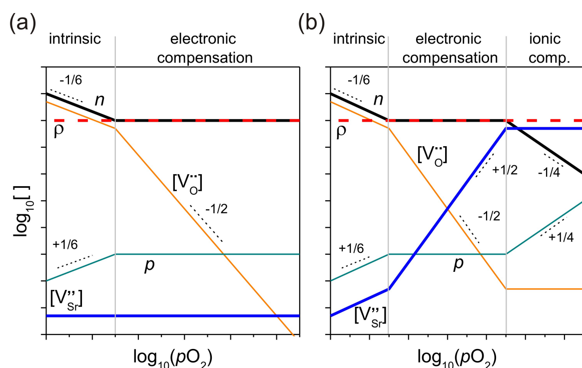

Fig. 1 Schematic illustration of equilibrium defect concentrations at the LAO/STO interface (in analogy to donor-doped STO) derived from defect chemistry calculations for (a) inactive and (b) active Schottky-equilibrium. Electrons (n), holes (p), oxygen vacancies ($V_O^{\bullet\bullet}$), and strontium vacancies (V_{Sr}'') compensate the interfacial charge associated with ρ. The characteristic decrease of n at high pO_2 appearing in (b) is a fingerprint for ionic charge compensation. For more details, please refer to Refs. 6,30.

ing behind cation vacancies. Thus, this compensation mechanism can take place only at elevated temperatures such as provided during growth or annealing procedures. V_{Sr}'' are then thermodynamically incorporated under the formation of SrO-secondary phases.[6,32] This process is particularly pronounced at high oxygen partial pressures. Comparing the two cases of inactive and active Schottky-equilibrium one finds the equilibrium defect concentrations as a function of pO_2 depicted in fig. 1 (a) and (b). For inactive Schottky-equilibrium, the electron density at the LAO/STO interface remains independent of pO_2 in oxidizing atmosphere (see fig. 1 (a)) because electrons are the only relevant defects compensating ρ. For an active Schottky-equilibrium, however, one finds a significant reduction of electronic conduction at high pO_2 because most of the charge is now compensated by an increasing amount of V_{Sr}'' (fig. 1 (b)).[30,32] This fingerprint of ionic charge compensation has been reported for both LAO/STO interfaces to STO single crystals and LAO/STO bilayers.[6] Moreover, associated SrO phases have recently been found on the surface of as-grown LAO/STO layers[33] indicating that Sr ions are mobile at typical growth conditions. As a consequence, charge compensation through V_{Sr}'' may be the main reason why typical electron densities found for LAO/STO interfaces can differ significantly from the value expected from the polarity catastrophe picture (cf. Ref. 34).

2.3 Defect engineering in thin film STO

The defect structure of thin films may differ strongly from the one of single crystals, because thin film growth is commonly a non-equilibrium process, whereas single crystal growth is performed much closer to thermodynamic equilibrium. This is the case particularly for thin films grown by PLD. For this reason, PLD-grown oxide thin films always exhibit a defect structure that is specific for the growth conditions. For STO thin films, the effect of PLD growth conditions on the defect structure has been investigated in great detail. It has been found that the cation stoichiometry, namely the Sr/Ti ratio, can vary significantly for STO thin films deposited with different ablation energies,[20,23,35] at different oxygen partial pressures,[36] or different target-to-substrate distances.[21] Moreover, the oxygen content of the STO thin films depends on the growth pressure and laser fluence.[22,37] In essence, the cation stoichiometry in STO thin films is determined by the balance between two competing processes, 1) preferential material ablation from the target and 2) preferential scattering of light elements within the plasma phase.[38] Generally, STO thin films are found to be Sr-rich for low laser fluences, while they tend to be Ti-rich for high laser fluences.[20,22–25]

As a result of non-stoichiometric growth, STO thin films incorporate defects, in particular vacancies on the sub-stoichiometric site. Both types of vacancies, V_{Sr}'' and V_{Ti}'''', cause an expansion of the STO unit cell volume due to the enhanced Coulomb repulsion between the unscreened oxygen anions surrounding the vacancy site.[39] For the case of Sr-rich films, non-stoichiometry is accommodated also by the insertion of Ruddlesden-Popper-like phases and Sr-rich antiphase boundaries rather than by titanium vacancies alone.[24,40] Such extended defect structures similarly result in a net expansion of the lattice. Therefore, the c-lattice constant of STO films or the actual elongation with respect to the bulk reference value, $\Delta c = (c - c_0)$, represents a qualitative measure of (non-) stoichiometry of a STO film. For a stoichiometric growth, a minimum Δc is expected.[41] In order to separate the lattice expansion caused by non-stoichiometry from general strain effects,[35] homoepitaxial growth is studied. Having calibrated the growth-control of the thin film cation stoichiometry, the results can then be transferred to the heteroepitaxial case as the stoichiometry-determining processes are mainly decoupled from the choice of the substrate material.

3 Experimental

3.1 Growth of LAO/STO bilayers with varied STO-cation stoichiometry

$LaAlO_3$ and $SrTiO_3$ thin films were deposited using PLD. As a reference sample set, 160 nm thick STO films were grown homoepitaxially on TiO_2-terminated STO single crystal substrates. The growth was conducted at a growth temperature $T_{dep} = 1070$ K, an oxygen pressure of $p_{dep}^{STO} = 0.1$ mbar, and a laser repetition rate of $f = 5$ s^{-1}. The laser fluence was set to

Nanoscale Accepted Manuscript

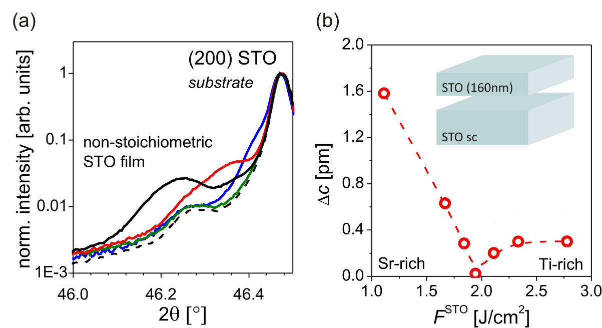

Fig. 2 (a) XRD scans around the (200) STO substrate peak for 160 nm thick homoepitaxial STO films. Laser fluence applied during growth: $F^{\mathrm{STO}} = 1.1$ J/cm^2 (black); 1.67 J/cm^2 (red); 1.9 J/cm^2 (green); 2.78 J/cm^2 (blue); The dashed line corresponds to the bare STO single crystal; (b) Corresponding *c*-lattice expansion of homoepitaxial STO as a function of F^{STO} (derived from (a)). The dashed line is a guide to the eye.

values between $1\ \mathrm{J/cm^2} < F^{\mathrm{STO}} < 3\ \mathrm{J/cm^2}$.

The *c*-lattice parameter of the *thick* homoepitaxial films was determined by means of X-ray diffraction experiments around the (200) STO substrate peak (fig. 2 (a)). For the lowest and the largest laser fluences a clear shoulder appears in the XRD-spectra indicating an elongated *c*-lattice parameter. Fig. 2 (b) depicts the extracted lattice expansion, Δc, as a function of applied laser fluence. A minimum lattice expansion is found at a laser fluence of $F^{\mathrm{STO}} = 1.9\ \mathrm{J/cm^2}$ indicating stoichiometric conditions, whereas the non-zero lattice expansion at lower and larger laser fluences indicates non-stochiometric growth. Comparison to various publications allows to conclude that the STO thin films become Sr-rich for $F^{\mathrm{STO}} < 1.9\ \mathrm{J/cm^2}$, while they become Ti-rich for $F^{\mathrm{STO}} > 1.9\ \mathrm{J/cm^2}$. At the chosen growth conditions, one can thus adjust the stoichiometry of the STO thin film from being Sr-rich to stoichiometric to Ti-rich by the variation of the laser energy. (However, Δc does not provide any quantitative information.)

Subsequently, heteroepitaxial STO thin films were grown on $(\mathrm{La,Sr})(\mathrm{Al,Ta})\mathrm{O_3}$ (LSAT) substrates using identical growth conditions providing the systematic variation of the STO thin films' cation stoichiometry. The growth was monitored using reflection high energy electron diffraction (RHEED). In order to accurately control the thickness of the STO layer, the laser repetition rate was reduced to $f = 1\ \mathrm{s^{-1}}$. The thickness of the heteroepitaxial layers was kept to 10 unit cells. In order to establish LAO/STO bilayers, the STO growth was directly followed by the growth of 10 unit cells LAO at $T_{\mathrm{dep}} = 1070$ K, $p_{\mathrm{dep}}^{\mathrm{LAO}} = 4 \times 10^{-5}$ mbar, $f = 1\ \mathrm{s^{-1}}$, and $F^{\mathrm{LAO}} = 1.4\ \mathrm{J/cm^2}$. All samples were cooled down to room temperature with a constant rate of 10 K/min in deposition pressure.

Using nanometer-thin heteroepitaxial STO films on LSAT substrates, we confine the electron transport at the LAO/STO interface to the stoichiometry-controlled STO and, at the same time, preserve layer-by-layer growth mode under any growth condition as depicted in fig. 3 (a). Clear RHEED intensity oscillations are observed during the growth of both the STO-layer and the LAO-layer (fig. 3 (b)) indicating layer-by-layer growth mode for the entire bilayer stack. In accordance with this, the step-terrace-structure of the substrate surface is conserved for all bilayer samples as verified by atomic force microscopy (fig. 3 (c-e)). This ensures an atomically defined LAO/STO interface in all bilayer samples. Using the insulating LSAT[6] as substrate and keeping the STO layer thickness small we furthermore avoid any major contribution of reduced STO interfering with interface conduction in our electrical measurements (even when working with extremely reducing conditions).[6,17]

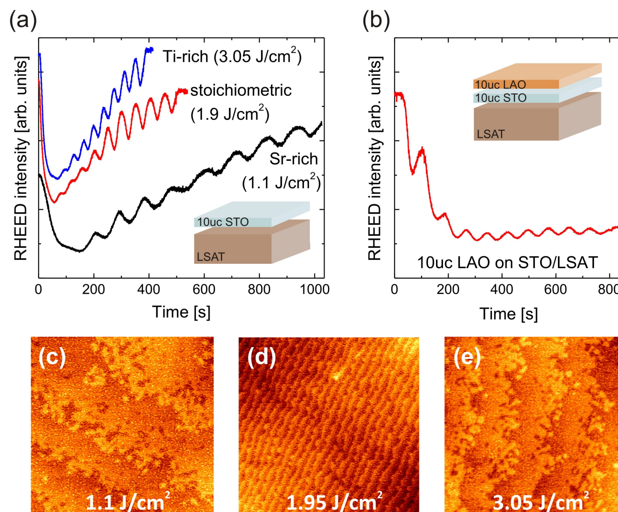

Fig. 3 Growth of LAO/STO bilayers: (a) Evolution of RHEED intensity during growth of 10 uc STO on LSAT at various laser fluences, (b) characteristic evolution of RHEED intensity during growth of 10 uc LAO on STO/LSAT. The RHEED intensity oscillations observed during grwoth at any growth conditions indicate layer-by-layer growth mode for all bilayer samples. (c)-(e) topography of LAO/STO bilayers obtained from atomic force microscopy ($5 \times 5\ \mu\mathrm{m}^2$). The clear terrace structure of the LSAT substrate is conserved during growth.

As the LAO-growth parameters were kept constant the LAO-stoichiometry is identical in all samples, so that any effect of LAO-stoichiometry is expected to be negligible.[37,42–44] The only parameter varied is the stoichiometry and thus the defect structure of the STO layer.

3.2 Electrical characterization

After growth, the LAO/STO-bilayer interfaces were contacted using ultrasonic Al-wire bonding. Temperature-dependent re-

Nanoscale Accepted Manuscript

This journal is © The Royal Society of Chemistry [year]

sistance measurements as well as Hall measurements were performed in van der Pauw geometry using a standard physical property measurement system (PPMS, Quantum Design) and a BIO RAD Hall system.
Electrical characterization in high-temperature equilibrium was conducted using a custom in-house system based on a yttria-stabilized ZrO_2-oxygen pump. The setup allows four-point measurements of the high temperature equilibrium conductance (HTEC) at temperatures between 900 K $< T <$ 1100 K in thermodynamic equilibrium with the surrounding atmosphere. The surrounding oxygen partial pressure, pO_2, can be controlled within the wide range of 10^{-23} bar $< pO_2 <$ 1 bar. At each individual equilibration temperature and pO_2, the resistance of the LAO/STO-bilayer samples was monitored until no further change was observed. In order to assure thermodynamic equilibrium, the samples were then kept in constant conditions for additional 1-2 hours. The HTEC was finally obtained from the slope of the linear I-V-curve recorded at each individual equilibration condition. Further details can be found in Refs. 5,45.

3.3 Quenching experiments

In order to set a thermodynamically defined equilibrium defect state of the LAO/STO bilayers, selected samples were annealed in defined gas flows supplied in a quartz glass tube. Subsequently, they were quickly quenched down to room temperature to preserve the defect state during cooling. A tube furnace was mounted such that it covered only a part of the quartz glass tube. This allows to quickly move the sample from the hot region (in the center of the furnace) into the cold region (outside the furnace). In the cold region, the samples cool down to room temperature within seconds ($\lesssim$ 10 s). Annealing procedures were performed at 1070 K for 6 hours in order to achieve thermodynamic equilibrium. The oxygen partial pressure of the gas atmosphere was varied using dry and wet 4%H_2/Ar gas mixture and Ar gas. An intermediate oxygen pressure was set using a commercial oxygen pump system (SGM5 EL, Zirox GmbH, Germany). The actual pO_2 was determined as listed in tab. 1 using an oxygen sensor (SGM7, Zirox GmbH, Germany) at the exhaust of the quartz glass tube.

Table 1 Oxygen partial pressure in various gas mixtures used for quenching experiments at 1070 K.

gas mixture	pO_2 / bar
dry 4%H_2/Ar	2×10^{-23}
wet 4%H_2/Ar	2×10^{-19}
SEMG5 (Ar)	$1\times10^{-13} - 1\times10^{-12}$
Ar	1×10^{-5}

4 Results

4.1 Transport properties of as-grown LAO/STO-bilayer-interfaces with varied STO cation stoichiometry

While all STO layers alone were found to be insulating, the growth of the LAO layer caused a drastic change from insulating behavior to significant in-plane conduction in all LAO/STO bilayer samples. Hence, the bilayer interfaces exhibit a similar reconstruction as LAO/STO interfaces to STO single crystals. The typical temperature dependence of the sheet resistance obtained for as-grown LAO/STO bilayers is displayed in fig. 4.
For the stoichiometric growth of STO, the LAO/STO bilayers typically exhibit a sheet resistance, R_S, in the range of 10 kΩ − 25 kΩ at room temperature. This is comparable to the values found for standard LAO/STO heterostructures comprising single crystal STO. The sheet resistance of the stoichiometric bilayer decreases with decreasing temperature generally reflecting a metallic temperature dependence. An resistance upturn is observed around 150 K, before R_S saturates at a value of several kilo ohms at temperatures below 50 K. This low temperature limiting value is about one to two orders of magnitude higher than the typical residual resistance observed for standard LAO/STO interfaces to single crystals (typically a few hundred ohms) hinting at an increased defect density in

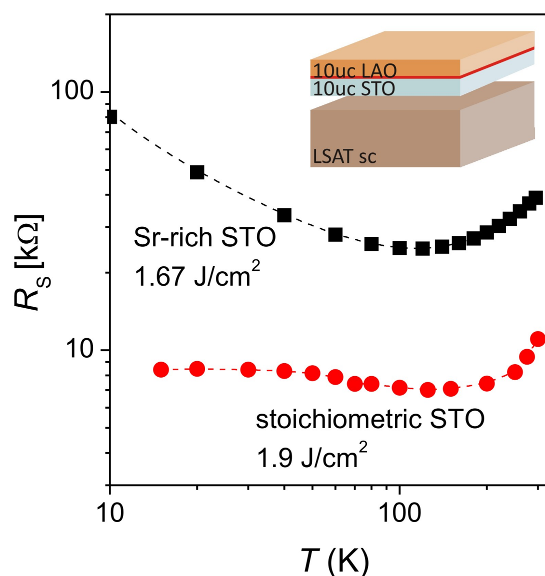

Fig. 4 Temperature dependence of the sheet resistance of LAO/STO bilayer interfaces comprising stoichiometric (red circles) and Sr-rich (black squares) STO thin films.

Nanoscale Accepted Manuscript

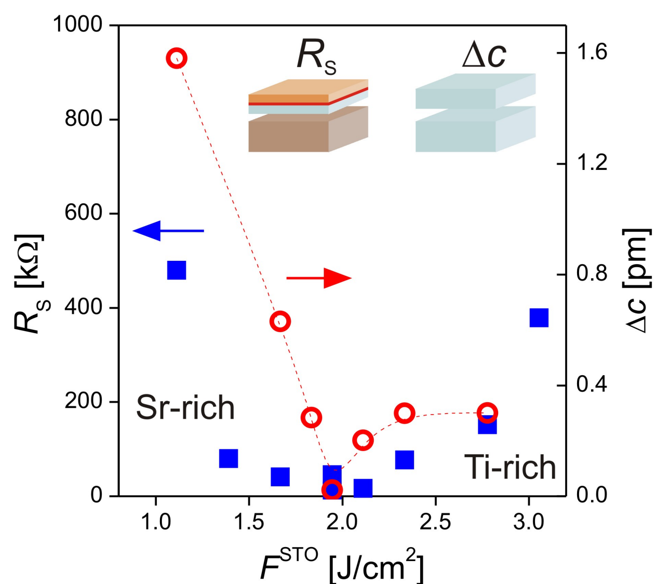

Fig. 5 Room temperature sheet resistance of LAO/STO bilayers with varied STO thin film stoichiometry (blue squares), c-lattice expansion of homoepitaxial STO thin films grown at various F^{STO} (red open circles). Δc is used as a qualitative measure of the cation stoichiometry of the STO layer adjacent to the LAO/STO bilayer interface.

the STO thin film as compared to a single crystal even under stoichiometric growth conditions. Such an increased density of defects in stoichiometric STO films was observed also by positron annihilation spectroscopy.[20]

In general, non-stoichiometric samples deliver higher sheet resistance values than stoichiometric samples as displayed in fig. 4 for an LAO/STO interface to slightly SrO-rich STO ($F^{\mathrm{STO}} = 1.67\ \mathrm{J/cm^2}$). Starting at 300 K, the non-stoichiometric sample exhibits a metallic temperature dependence. Below 120 K, the resistance shows an upturn and increases constantly indicating an even more pronounced effect of defect scattering or carrier freeze-out than for the stoichiometric case.

Fig. 5 depicts the room temperature sheet resistance, R_{S}, of the as-grown LAO/STO bilayers as a function of the laser fluence applied during growth of the STO layer. For comparison, the c-lattice expansion of the homoepitaxial reference samples - used as a measure of the cation non-stoichiometry of the STO films - is added to the plot. Obviously, R_{S} exhibits a minimum for the heterostructures with almost stoichiometric STO layers indicated by the vanishing c-lattice expansion of the homoepitaxial films at $F^{\mathrm{STO}} = 1.9\ \mathrm{J/cm^2}$. For Sr-rich as well as Ti-rich STO layers, the sheet resistance of the LAO/STO bilayer increases with increasing non-stoichiometry, finally reaching several hundreds of kilo-ohms at $F^{\mathrm{STO}} = 1.1\ \mathrm{J/cm^2}$ and at $F^{\mathrm{STO}} = 3.05\ \mathrm{J/cm^2}$, respectively. Thus, the interface conduction is affected for both types of non-stoichiometry, Ti-rich composition and Sr-rich composition. In fact, the sheet resistance of the LAO/STO interface can be tailored and controlled by the (non-) stoichiometry of the involved STO layer.

As discussed earlier, one way to accommodate non-stoichiometry is the incorporation of cation vacancies on the under-stoichiometric site. Being acceptor-type, these cation vacancies are expected to (partially) suppress the donor-type interface conduction, provided that their concentration is sufficiently high. In a simple picture, one could expect an effective charge density

$$\rho_{\mathrm{eff}} = \rho - 4\left[V_{\mathrm{Sr}}''\right]_{\mathrm{inherent}} - 2\left[V_{\mathrm{Ti}}''''\right]_{\mathrm{inherent}}$$

for the LAO/STO interface to a non-stoichiometric STO layer resulting in a decreased sheet electron density, $n_{\mathrm{S}} = \rho_{\mathrm{eff}} \times t$. However, at the same time it is expected that inherent defects - vacancies as well as extended defects - enhance electron scattering and hinder electron transport along the interface. Hence, μ_n could be decreased in the non-stoichiometric bilayers, too. Both scenarios are consistent with the resistance behavior shown in fig. 5.

To clarify this point, several samples were investigated by Hall measurements at 300 K. The results are presented in fig. 6. The non-stoichiometry of the STO layer primarily influ-

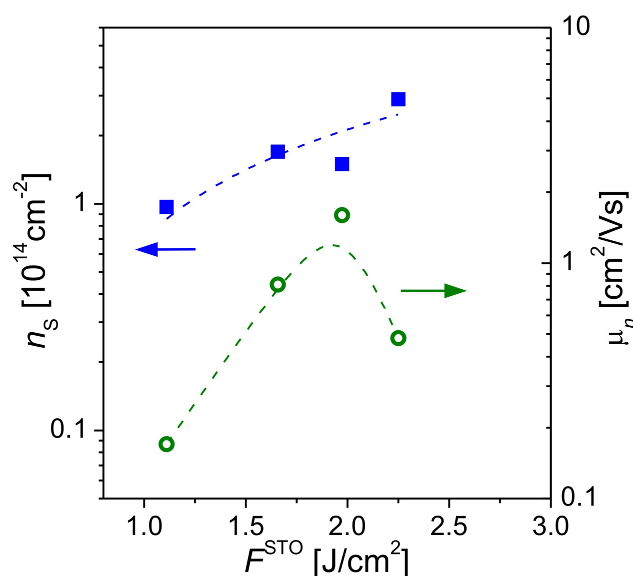

Fig. 6 Room temperature Hall data obtained for as grown LAO/STO bilayers with varied STO stoichiometry. The dashed lines are guides to the eye.

This journal is © The Royal Society of Chemistry [year]

Nanoscale Accepted Manuscript

ences the electron mobility which exhibits an opposite dependence on laser fluence as R_S. For a stoichiometric growth of the STO layer, μ_n reaches its maximum value of 1.6 cm^2/Vs. For Sr-rich and Ti-rich growth of the STO layer, the mobility is reduced by up to one order of magnitude. In contrast to that, n_S is for all samples of the same order of magnitude ($\approx 10^{14}$ cm^{-2}), while it shows a slight tendency to increase with increasing laser fluence (within a factor of 3). The lowest sheet carrier density is found for the interface to the Sr-rich STO layer and the highest sheet carrier density is found for the interface to the Ti-rich STO layer.

In bulk STO (or standard LAO/STO heterostructures), μ_n at room temperature is typically limited by phonon scattering yielding $\mu_{ph} \approx 5-10$ cm^2/Vs.[32] Hence, the low mobility values ($\mu_n \lesssim 1-2$ cm^2/Vs) obtained for LAO/STO bilayers in this study as well as in literature[16,17] indicate that defect scattering affects and ultimately limits μ_n in the thin film LAO/STO interface samples even at 300 K. This is the case also for stoichiometric STO thin film composition. Such an effect of μ_n being limited by cationic defects has been reported for donor-doped STO thin films, too.[46] The further decrease in mobility when tuning the STO stoichiometry indicate that non-stoichiometry of the STO layer causes a further increase in the concentration of scatter centers, i.e. defects, in the vicinity of the LAO/STO interface.

Generally, data taken for differently grown samples refer to non-equilibrium states. Therefore, the trend found for n_S may be due to the fact that the oxidation state of the deposited thin films depends on the actual laser fluence applied during STO growth,[22,37] i.e. oxygen loads and associated defect states may slightly differ from sample to sample. It may also be related to a partial change of the surface termination during STO growth as recently reported by Reinle-Schmitt et al..[47] This effect should be most pronounced for SrO-rich growth. However, a termination effect alone cannot account for the observed maximum of the mobility for stoichiometric growth conditions as one in this case would rather expect a monotonous trend when tuning from Sr-rich to Ti-rich STO composition.

4.2 High temperature conductance in equilibrium with the surrounding atmosphere

In high temperature equilibrium experiments, it is monitored how the LAO/STO bilayer reacts to - and equilibrates with - a systematically varied pO_2 in its surrounding. From the characteristic behavior it can be deduced which defect equilibria define the thermodynamics of the interface and how charge compensation is accomplished. Any non-equilibrium effects vanish in high temperature equilibrium.

Fig. 7 presents the HTEC characteristics of LAO/STO bilayers on LSAT for (a) a stoichiometric STO layer, (b) a Ti-rich STO layer, and (c) a Sr-rich STO layer. For clarity, fig. 7(d) compares the HTEC characteristics of the three samples at an equilibration temperature of 950 K. All samples show a similar behavior. Two characteristic features can be unambiguously assigned to interface conduction:[6] 1) a conductance plateau, this is the HTEC's tendency to saturate in reducing atmosphere, and 2) a temperature-activated decrease in conductance at intermediate oxygen partial pressures. In constrast, the increase in conductance (3) observed at $pO_2 \gtrsim 10^{-8}$ bar is due to conduction through the LSAT substrate as discussed in Ref. 6. As argued therein and in section 2.2, feature 1) can be attributed to electronic compensation, $\rho_{eff} = n$, while feature 2) results from ionic charge compensation due to the insertion of Sr-vacancies via the Schottky-equilibrium, $\rho_{eff} = 2[V''_{Sr}]$.

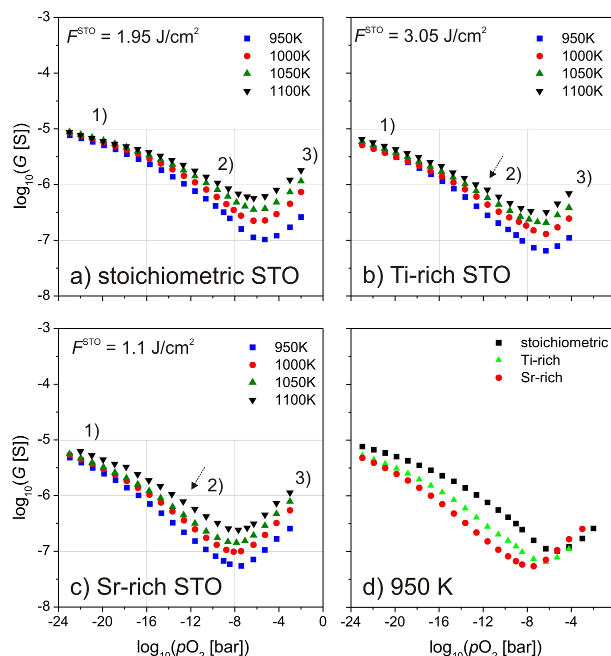

Fig. 7 HTEC of LAO/STO/LSAT heterostructures (G) comprising (a) stoichiometric STO, (b) Ti-rich STO, and (c) Sr-rich STO. (d) comparison of the HTEC characteristics of all samples for the equilibration temperature of 950 K.

In essence, a comparable donor-type conduction mechanism as well as a comparable ionic charge compensation mechanism can be assumed for all samples. The conductance plateau is less pronounced for the non-stoichiometric samples than for the stoichiometric sample. In fact, it is slightly shifted downwards. This might indicate a slightly lower ρ_{eff} in the non-stoichiometric samples, provided that the electron mobility in this high temperature regime is identical for all samples. Applying a literature value for μ_n obtained for bulk STO at high temperatures,[32] one receives an equilibrium sheet carrier den-

Nanoscale Accepted Manuscript

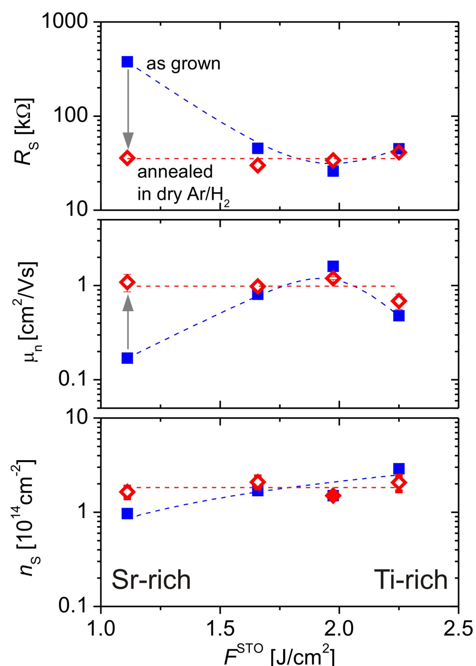

Fig. 8 Room temperature sheet resistance (top), electron mobility (middle), and sheet carrier density (bottom) obtained for LAO/STO bilayers comprising STO thin films with varied cation stoichiometry. Blue squares refer to the as-grown state, red diamonds to the quenched state after equilibration in dry 4%H_2/Ar gas mixture ($pO_2 \approx 2 \times 10^{-23}$ bar). The dashed lines are guides to the eye.

sity, $n_S = G/e\mu_n$, of about 1×10^{14} cm^{-2} in the electronic compensation regime (reducing atmosphere).

In the intermediate pressure range, the characteristics of the non-stoichiometric samples are shifted towards lower oxygen partial pressures and lower conductance values, too (as indicated by the arrows in figs. 7 (b), (c)). These shifts become more obvious in direct comparison (fig. 7(d)). As this intermediate pO_2 region was identified with a Schottky-like compensation mechanism,[6] the shift of the conductance characteristics indicates a dependence of the associated thermodynamics - in particular the one of the Schottky equilibrium - on the actual inherent stoichiometry and defect structure of the STO layer.

(One may further expect that an increased concentration of cation vacancies in (non-stoichiometric) thin film STO comes along with facilitated cation diffusion. However, this refers to dynamic processes not accessible in HTEC measurements.)

4.3 Quenching experiments

The defect chemical state obtained in high temperature equilibrium can be conserved by rapidly cooling the samples down to room temperature. This is done by quenching experiments where the sample is cooled down to room temperature from a defined equilibrium state within a few seconds. By quenching, the defect equilibria freeze almost instantly, and an adjustment of the defect concentrations during cooling is effectively prevented.[48] As a consequence, the concentrations of ionic defects at room temperature are similar to the ones achieved during high temperature equilibration. Similarly, the high temperature electron density is expected to be conserved at low temperatures, too. In the quenched state, the effect of defect structure on the transport can thus be studied using standard room temperature equipment.

In order to estimate ρ_{eff} in the LAO/STO bilayers with different STO stoichiometry, the samples were equilibrated in reducing atmospheres where charge compensation is mostly electronic. Fig. 8 shows the sheet resistance, electron mobility, and sheet electron density in the quenched state after 6 hours of equilibration at 1070 K in reducing 4%H_2/Ar atmosphere. The clear dependence of the sheet resistance (top) and the electron mobility (middle) on the inherent cation stoichiometry of the as-grown samples tends to even out after the equilibration in the plateau-region. In particular, the electron mobility is increased in the non-stoichiometric samples and almost reaches a common level of about 1 cm^2/Vs independent of the particular inherent defect configuration. This indicates, that the presumed additional defects at the LAO/STO interface to non-stoichiometric STO layers can be healed - at least partially - by the high temperature treatment. Thus, the enhanced scattering processes in the as-grown non-stoichiometric samples may be caused not only by inherent cationic point defects, but also by associated extended structural defects incorporated during non-stoichiometric growth.[24,25,40] This healing effect is most pronounced for bilayers comprising Sr-rich STO which is known to incorporate Ruddlesden-Popper phases to accommodate non-stoichiometry. These extended defects seem to partially reorganize during the thermal treatment causing the recovery of μ_n.

The sheet carrier density at the LAO/STO interface (bottom panel) evens out after the equilibration, too. Hence, there is only a minor effect of inherent cation vacancies on ρ_{eff}, i.e. the background acceptor doping by cation vacancies is small compared to ρ. This sets an upper limit for the growth-induced inherent cation vacancy concentrations of the non-stoichiometric STO layers

$$\rho_{\text{eff}} \approx \rho >> 4\left[V''_{\text{Sr}}\right]_{\text{inherent}} + 2\left[V''''_{\text{Ti}}\right]_{\text{inherent}}$$

yielding inherent cation vacancy concentrations below 1at% for the investigated samples. The initial tendency in the as-grown samples of an increasing electron density with increasing laser fluence thus may result from deviating non-equilibrium states (and oxidation states) of the samples generated during the growth. One obtains $n_S \approx 2 \times 10^{14}$ cm^{-2} for all samples which agrees well with the values estimated in high

 This journal is © The Royal Society of Chemistry [year]

Nanoscale Accepted Manuscript

temperature equilibrium (cf. sec. 4.2). We can exclude here that the observed conductivity after annealing in 4%H_2/Ar arises from a reduction of the 10 uc thick STO layer only. Although oxygen vacancy concentration and thus electronic conductivity in thin film STO is generally enhanced compared to bulk[31], the observed in-plane conductance of the annealed LAO/STO bilayers is much larger than that expected for a highly reduced, 4nm-thick STO thin film (see Refs. 6,31). This has been checked experimentally by quenching bare STO thin films in a similar atmosphere. All of these samples were found insulating at room temperature. Thus, the conductance of the LAO/STO bilayers observed after quenching can be unambiguously attributed to interfacial electron transport.

In order to further probe the influence of the Schottky equilibrium on the electrical properties of LAO/STO interface, 4 samples cut from the same LAO/STO/LSAT heterostructure were equilibrated for 6 hours at 1070 K in various atmospheres before quenching the achieved defect state down to room temperature. Initially, the LAO/STO/LSAT sample had a sheet resistance of about 100 kΩ corresponding to a sheet carrier density of 2×10^{14} cm^{-2} and an electron mobility of 0.35 cm^2/Vs. The low initial mobility indicated a slight non-stoichiometry of the subjacent STO layer, as discussed above. The results of the quenching experiments are displayed in fig. 9. After equilibration, the carrier density of the samples which had been annealed in wet and dry 4%H_2/Ar gas mixture did not differ significantly from the initial value. By contrast, the samples which had been equilibrated in higher oxygen partial pressure showed a considerable decrease in the carrier density. For an oxygen partial pressure of about 10^{-12} bar, the sheet carrier density decreased by one order of magnitude to 2×10^{13} cm^{-2}. The sample annealed in Ar gas even exhibited insulating behavior after the equilibration. The mobility of all samples - showing a measurable conductance - increased after the heat treatment. Thus, the presumed healing effect takes place independent of the actual pO_2 during heat treatment.

The dependence of the sheet carrier density on the equilibration atmosphere corresponds well with the predicted equilibrium values displayed in fig. 7 ($n_S = G/e\mu_n$). For reducing conditions, a constant plateau-like behavior was expected due to the electronic compensation of the interface charge. For intermediate and oxidizing conditions, a decrease of n_S was expected due to the ionic compensation of ρ_{eff} by V''_{Sr} induced via the Schottky-equilibrium (see fig. 1(b)). After annealing in Ar atmosphere ($pO_2 \approx 10^{-5}$ bar) ionic charge compensation through strontium vacancies is as pronounced as the electron density at the LAO/STO bilayer interface drops below the room temperature conduction threshold resulting in insulating behavior.

Interestingly, the sheet carrier density obtained for the *as-grown* LAO/STO bilayers corresponds with the carrier densities obtained for samples *equilibrated* in very reducing atmosphere ($pO_2 \lesssim 10^{-19}$ bar). Considering that the nominal oxygen background pressure in the PLD chamber was $p^{LAO}_{dep} = 4 \times 10^{-8}$ bar in the final stage of the fabrication process, this emphasizes that the PLD growth process and the resulting defect state is far from thermodynamic equilibrium. During growth, the sample is driven into a *non-equilibrium* defect state which *in equilibrium* corresponds to much more reducing atmosphere than expected from the nominal growth pressure. A similar effect can be concluded from the growth-induced reduction of STO substrates reported in Ref. 49.

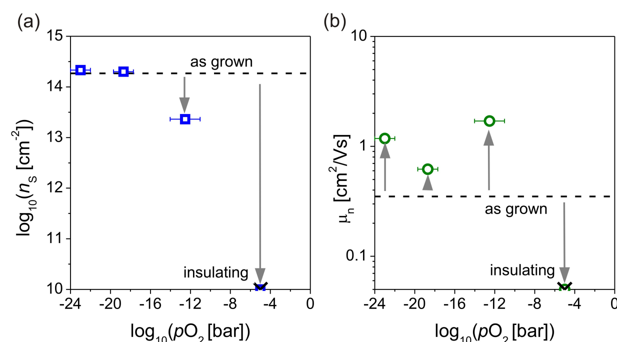

Fig. 9 Room temperature Hall data obtained for a quenched LAO/STO bilayer after equilibration in various pO_2 (cf. tab. 1 for details on the used gas mixtures). After equilibration at $pO_2 = 1 \times 10^{-5}$ bar, the sample turned insulating and no data could be recorded (indicated by the black crosses). The dashed lines indicate as grown values.

5 Conclusions

In this study, the influence of the STO cation stoichiometry on the electronic properties of the LAO/STO interface has been addressed. Following thermodynamic considerations, it has been emphasized that - irrespective of the particular donor-type doping mechanism (polarity catastrophe, chemical doping, etc.) - all thermodynamic processes, decisive defect species and charge compensation mechanisms relevant in bulk STO have to be considered for the LAO/STO interface, too. This includes electronic and ionic compensation of the space charge at the interface. Cation vacancies, in particular V''_{Sr}, can form at LAO/STO interfaces and serve as charge compensating defects. The understanding of these thermodynamic processes enable a control of the electronic properties of complex transition metal oxide interfaces, but at the same time they point out severe limits of the performance of these electron systems.

As shown, as-grown LAO/STO heterostructure devices obtained by PLD exhibit a drastic non-equilibrium defect structure involving both oxygen and cation species. Understanding and controlling this defect structure is still a key issue in the

Nanoscale Accepted Manuscript

field of oxide heterostructures and interfaces.

In this context, we discussed two possible ways of manipulating and controlling the cation stoichiometry of the STO layer in the vicinity of the LAO/STO interface. Both strategies, 1) growth-induced variation of the cation stoichiometry (a defect engineering process) and 2) thermal insertion of strontium vacancies via the Schottky reaction (a thermodynamical process), have been shown to modify the transport properties of the LAO/STO interface.

A variation of the STO growth parameters primarily tailors the electron mobility at the LAO/STO interface due to the incorporation of point defects as well as extended defects in non-stoichiometric STO thin films. However, the amount of acceptor-type point defects induced during growth seems insufficient to alter the effective charge density ρ_{eff} and the resulting electron concentration at the LAO/STO interface.

By contrast, thermal annealing in various oxygen partial pressures varies the electron density at the LAO/STO interface. In this case, charge compensation shifts from being mostly electronic in reducing atmosphere to being mostly ionic in oxidizing atmosphere. In addition, high temperature annealing leads to an increase in mobility. This indicates that extended structural defects such Ruddlesden-Popper-like defects induced during non-stoichiometric growth contribute to electron scattering and that these can rearrange and heal during a thermal treatment.

The results underline the direct interrelation between interfacial conductivity and cationic defects in the STO layer adjacent to the LAO/STO interface. Such defects evidently exist even in nominally stoichiometric STO and limit the electron mobility which at room temperature did not exceed $1-2\ \mathrm{cm}^2/\mathrm{Vs}$ for any bilayer sample. In order to achieve sufficient performance of thin film LAO/STO devices or superlattices with multiple conducting interfaces, it is thus necessary to further decrease the defect concentrations in thin film STO beyond the stoichiometry control presented in this study. In order to overcome this challenging task we suggest to use of extreme growth temperatures[46,50] or to utilize alternative growth techniques.[51]

References

1 A. Ohtomo and H. Y. Hwang, *Nature*, 2004, **427**, 423–426.
2 W. Harrison, E. Kraut, J. Waldrop and R. Grant, *Physical Review B*, 1978, **18**, 4402–4410.
3 D. G. Schlom and J. Mannhart, *Nature Materials*, 2011, **10**, 168–169.
4 H. Y. Hwang, Y. Iwasa, M. Kawasaki, B. Keimer, N. Nagaosa and Y. Tokura, *Nature Materials*, 2012, **11**, 103–113.
5 F. Gunkel, S. Hoffmann-Eifert, R. Dittmann, S. Mi, C. Jia, P. Meuffels and R. Waser, *Applied Physics Letters*, 2010, **97**, 12103/1–3.
6 F. Gunkel, P. Brinks, S. Hoffmann-Eifert, R. Dittmann, M. Huijben, J. E. Kleibeuker, G. Koster, G. Rijnders and R. Waser, *Applied Physics Letters*, 2012, **100**, 052103.
7 N. Nakagawa, H. Y. Hwang and D. A. Muller, *Nature Materials*, 2006, **5**, 204–9.
8 G. Herranz, M. Basletic, M. Bibes, C. Carretero, E. Tafra, E. Jacquet, K. Bouzehouane, C. Deranlot, A. Hamzic, J. M. Broto, A. Barthelemy and A. Fert, *Physical Review Letters*, 2007, **98**, 216803/1–4.
9 W. Siemons, G. Koster, H. Yamamoto, T. H. Geballe, D. H. A. Blank and M. R. Beasley, *Physical Review B: Condensed Matter*, 2007, **76**, 155111/1–.
10 P. R. Willmott, S. A. Pauli, R. Herger, C. M. Schlepuetz, D. Martoccia, B. D. Patterson, B. Delley, R. Clarke, D. Kumah, C. Cionca and Y. Yacoby, *Physical Review Letters*, 2007, **99**, 155502/1–.
11 L. Houben, M. Heidelmann and F. Gunkel, *Micron*, 2012, **43**, 532–537.
12 S. A. Chambers, *Surface Science*, 2011, **605**, 1133–1140.
13 L. Qiao, T. C. Droubay, T. Varga, M. E. Bowden, V. Shutthanandan, Z. Zhu, T. C. Kaspar and S. A. Chambers, *Physical Review B*, 2011, **83**, 085408.
14 A. Kalabukhov, R. Gunnarsson, J. Borjesson, E. Olsson, T. Claeson and D. Winkler, *Phyical Review B*, 2007, **75**, 121404/1–4.
15 A. S. Kalabukhov, Y. A. Boikov, I. T. Serenkov, V. I. Sakharov, V. N. Popok, R. Gunnarsson, J. Borjesson, N. Ljustina, E. Olsson, D. Winkler and T. Claeson, *Physical Review Letters*, 2009, **103**, 146101/1–4.
16 J. W. Park, D. F. Bogorin, C. Cen, D. A. Felker, Y. Zhang, C. T. Nelson, C. W. Bark, C. M. Folkman, X. Q. Pan, M. S. Rzchowski, J. Levy and C. B. Eom, *Nature Communications*, 2010, **1**, 94/1–6.
17 P. Brinks, W. Siemons, J. E. Kleibeuker, G. Koster, G. Rijnders and M. Huijben, *Applied Physics Letters*, 2011, **98**, 242904/1–3.
18 M. L. Reinle-Schmitt, C. Cancellieri, A. Cavallaro, G. F. Harrington, S. J. Leake, E. Pomjakushina, J. A. Kilner and P. R. Willmott, *Nanoscale*, 2014, **6**, 2598–2602.
19 C. W. Bark, D. A. Felker, Y. Wang, Y. Zhang, H. W. Jang, C. M. Folkman, J. W. Park, S. H. Baek, H. Zhou, D. D. Fong, X. Q. Pan, E. Y. Tsymbal, M. S. Rzchowski and C. B. Eom, *Proceedings of the National Academy of Sciences of the United States of America*, 2011, **108**, 4720–4724.
20 D. J. Keeble, S. Wicklein, R. Dittmann, L. Ravelli, R. A. Mackie and W. Egger, *Physical Review Letters*, 2010, **105**, 226102.
21 S. Wicklein, A. Sambri, S. Amoruso, X. Wang, R. Bruzzese *et al.*, *Applied Physics Letters*, 2012, **101**, 131601.
22 T. Ohnishi, K. Shibuya, T. Yamamoto and M. Lippmaa, *Journal of Applied Physics*, 2008, **103**, 103703.
23 T. Ohnishi, M. Lippmaa, T. Yamamoto, S. Meguro and H. Koinuma, *Applied Physics Letters*, 2005, **87**, 241919.
24 Y. Tokuda, S. Kobayashi, T. Ohnishi, T. Mizoguchi, N. Shibata, Y. Ikuhara and T. Yamamoto, *Applied Physics Letters*, 2011, **99**, 173109.
25 Y. Tokuda, S. Kobayashi, T. Ohnishi, T. Mizoguchi, N. Shibata, Y. Ikuhara and T. Yamamoto, *Applied Physics Letters*, 2011, **99**, 033110.
26 T. Fix, F. Schoofs, J. L. MacManus-Driscoll and M. G. Blamire, *Applied Physics Letters*, 2010, **97**, 072110.
27 T. Fix, F. Schoofs, J. L. MacManus-Driscoll and M. G. Blamire, *Physical Review Letters*, 2009, **103**, 166802.
28 F. Kroger and H. Vink, *Solid State Physics-Advances in Reasearch and Applications*, 1956, **3**, 307–435.
29 M. Akthar, Z. Akthar, R. Jackson and C. Catlow, *Journal of the American Ceramic Society*, 1995, **78**, 421–428.
30 D. M. Smyth, *The Defect Chemistry of Metal Oxides*, Oxford University Press, New York, 2000.
31 R. A. De Souza, F. Gunkel, S. Hoffmann-Eifert and R. Dittmann, *Phys. Rev. B*, 2014, **89**, 241401.
32 R. Moos and K. H. Haerdtl, *Journal of American Ceramic Society*, 1997, **80**, 2549–2562.
33 U. Treske, N. Heming, M. Knupfer, B. Bchner, A. Koitzsch, E. Di Gennaro, U. Scotti di Uccio, F. Miletto Granozio and S. Krause, *APL Materials*, 2014, **2**, –.

Nanoscale Accepted Manuscript

This journal is © The Royal Society of Chemistry [year]

34 J. A. Bert, B. Kalisky, C. Bell, M. Kim, Y. Hikita, H. Y. Hwang and K. A. Moler, *Nature Physics*, 2011, **7**, 767–771.

35 E. Breckenfeld, R. Wilson, J. Karthik, A. R. Damodaran, D. G. Cahill and L. W. Martin, *Chem. Mater.*, 2012, **24**, 331–337.

36 G. Z. Liu, Q. Y. Lei and X. X. Xi, *Applied Physics Letters*, 2012, **100**, 202902.

37 E. Breckenfeld, N. Bronn, J. Karthik, A. R. Damodaran, S. Lee, N. Mason and L. W. Martin, *Phys. Rev. Lett.*, 2013, **110**, 196804/1–.

38 C. Xu, S. Wicklein, A. Sambri, S. Amoruso, M. Moors and R. Dittmann, *J. Phys. D Appl. Phys.*, 2014, **47**, 34009/1–.

39 D. A. Freedman, D. Roundy and T. A. Arias, *Physical Review B*, 2009, **80**, 064108.

40 D. Keeble, S. Wicklein, L. Jin, C. L. Jia, W. Egger and R. Dittmann, *Phys. Rev. B: Condens. Matter*, 2013, **87**, 11.

41 J. M. LeBeau, R. Engel-Herbert, B. Jalan, J. Cagnon, P. Moetakef, S. Stemmer and G. B. Stephenson, *Applied Physics Letters*, 2009, **95**, 142905.

42 M. P. Warusawithana, C. Richter, J. A. Mundy, P. Roy, J. Ludwig, S. Paetel, T. Heeg, A. A. Pawlicki, L. F. Kourkoutis, M. Zheng, M. Lee, B. Mulcahy, W. Zander, Y. Zhu, J. Schubert, J. N. Eckstein, D. A. Muller, C. S. Hellberg, J. Mannhart and D. G. Schlom, *Nat. Commun.*, 2013, **4**, 2351/1–9.

43 H. K. Sato, C. Bell, Y. Hikita and H. Y. Hwang, *Appl. Phys. Lett.*, 2013, **102**, 251602/1–4.

44 F. Gunkel, K. Skaja, A. Shkabko, R. Dittmann, S. Hoffmann-Eifert and R. Waser, *Appl. Phys. Lett.*, 2013, **102**, 71601/1–4.

45 C. Ohly, S. Hoffmann-Eifert, X. Guo, J. Schubert and R. Waser, *Journal of American Ceramic Society*, 2006, **89**, 2845 – 2852.

46 Y. Kozuka, Y. Hikita, C. Bell and H. Y. Hwang, *Applied Physics Letters*, 2010, **97**, 12107/1–3.

47 M. L. Reinle-Schmitt, C. Cancellieri, A. Cavallaro, G. F. Harrington, S. J. Leake, E. Pomjakushina, J. A. Kilner and P. R. Willmott, *Nanoscale*, 2014, **6**, 2598–2602.

48 R. Waser, *Journal of American Ceramic Society*, 1991, **74**, 1934–1940.

49 M. L. Scullin, J. Ravichandran, C. Yu, M. Huijben, J. Seidel, A. Majumdar and R. Ramesh, *Acta Materialia*, 2010, **58**, 457–463.

50 D. Li, S. Gariglio, C. Cancellieri, A. Fete, D. Stornaiuolo and J.-M. Triscone, *APL MATERIALS*, 2014, **2**, 012102.

51 J. Son, P. Moetakef, B. Jalan, O. Bierwagen, N. J. Wright, R. Engel-Herbert and S. Stemmer, *Nature Materials*, 2010, **9**, 482–484.

Nanoscale Accepted Manuscript